NOTES AND CORRESPONDENCE

NEOPLANTA: A Short Description of the First Serbian UV Index Model

S. MALINOVIC

University Center for Meteorology and Environmental Modelling, University of Novi Sad, Novi Sad, Serbia

D. T. MIHAILOVIC

Faculty of Agriculture, University of Novi Sad, Novi Sad, Serbia

D. KAPOR AND Z. MIJATOVIC

Department of Physics, Faculty of Natural Sciences and Mathematics, University of Novi Sad, Novi Sad, Serbia

I. D. ARSENIC

Faculty of Agriculture, University of Novi Sad, Novi Sad, Serbia

(Manuscript received 29 June 2005, in final form 26 October 2005)

ABSTRACT

A numerical model called "NEOPLANTA" for estimating solar UV irradiance and UV index under cloud-free conditions is being developed and tested at the University of Novi Sad in Serbia. In this paper, the model features, calculation procedure, and input parameters are described. Effects of the absorption of UV radiation by O_3, SO_2, and NO_2 and absorption and scattering by aerosol as well as the air molecules in the atmosphere are included. The performance of the model has been tested with respect to its capability of UV index, which is a weighted integral between 280 and 400 nm of the solar irradiance reaching the ground. For this test 10-day data measured during the spring and summer in 2003, 2004, and 2005 are used. Data are recorded by the Yankee UVB-1 biometer located at the Novi Sad university campus (45.33°N, 19.85°E; 84 m MSL). Error analyses indicate that the modeled values agree well with the observations.

1. Introduction

Over the past decades, a depletion of stratospheric ozone has been detected, raising concern about increased surface UV radiation levels (Glandorf et al. 2005). For that reason, scientists have placed a large emphasis on monitoring UV radiation and estimation procedures (Zerefos 2002; Koepke et al. 1998; Madronich et al. 1998; WMO 2003; McKenzie et al. 2003; among others). The World Meteorological Organization (WMO) and World Health Organization (WHO) proposed the UV index as a quantity for biologically relevant solar UV radiation (WMO 1997). The UV index forecast is based on the use of radiative transfer models in connection with predicted values of the relevant atmospheric parameters. Spectral irradiance models can be classified into three basic categories: 1) multiple scattering spectral models that integrate radiance over the whole sky vault (Rozanov et al. 1997; Kneizys et al. 1988; Schwander et al. 2001); 2) fast spectral models that are analytical simplifications of the radiative transfer equation (Gueymard 1995; Bird and Riordan 1986; Diffey 1977); and 3) empirical models that compute UV irradiances based on fits of several years of UV observations (Burrows et al. 1994; Koepke et al. 1998). A comparison between several models belonging to these classes has been performed by Koepke et al. (1998). The model "NEOPLANTA," by its characteristics, can be classified into the first two types. It

Corresponding author address: Slavica Malinovic, University Center for Meteorology and Environmental Modelling, University of Novi Sad, 21000 Novi Sad, Serbia.
E-mail: slavicans@polj.ns.ac.yu

was developed at the University of Novi Sad (Malinovic 2003) as the first original model in Serbia.

2. Model description

The numerical model NEOPLANTA computes the solar direct and diffuse UV irradiances under cloud-free conditions for the wavelength range 280–400 nm (with 1-nm resolution) as well as the UV index. The effects of O_3, SO_2, NO_2, aerosols, and nine different ground surface types on UV radiation are included. The model calculates instantaneous spectral irradiance for a given solar zenith angle, but there is also a possibility for calculation of the UV index for the whole day at half-hour intervals from sunrise to sunset. Also, there is the possibility of taking into account daylight saving time. The atmosphere is divided into several parallel layers (maximum 40) in the model. It is assumed that the layers are homogeneous with constant values of meteorological parameters. The vertical resolution of the model is 1 km for altitudes below 25 km and 5 km above this height. The upper boundary of the highest layer in the model is 100 km. The model uses standard atmosphere meteorological profiles. However, there is also an option of including the real-time meteorological data profiles from the high-level resolution mesoscale models.

The required input parameters are the local geographic coordinates and time or solar zenith angle, altitude, spectral albedo, and the total amount of gases. The model includes its own vertical gas profiles (Ruggaber et al. 1994) and extinction cross sections (Burrows et al. 1999; Bogumil et al. 2000), extraterrestrial solar irradiance shifted to terrestrial wavelength (Koepke et al. 1998), aerosol optical properties for 10 different aerosol types (Hess et al. 1998), and spectral albedo for nine different ground surface types (Ruggaber et al. 1994). Output data are spectral direct, diffuse, and global irradiance divided into the UV-A (320–400 nm) and UV-B (280–320 nm) part of the spectrum, biologically active UV irradiance calculated using the erythemal action spectrum by McKinley and Diffey (1987), UV index, spectral optical depth, and spectral transmittance for each atmospheric component. All outputs are computed at the lower boundary of each layer.

a. Direct radiation

Calculation of the direct part of radiation is carried out by the Beer–Lambert law. The direct irradiance at wavelength λ received at the ground level by a unit area is given by

$$I_{\mathrm{dir}}(\lambda) = I_0(\lambda)T(\lambda), \tag{1}$$

where $I_0(\lambda)$ is the extraterrestrial irradiance corrected for the actual sun–Earth distance and $T(\lambda)$ is the total transmittance. The ellipticity of Earth's orbit around the sun is considered as a correction to the extraterrestrial solar spectrum $I_\infty(\lambda)$ by multiplication with an actual sun–Earth distance factor D (Spencer 1971):

$$I_0(\lambda) = I_\infty(\lambda)D\cos\theta. \tag{2}$$

The total transmittance includes different extinction processes as

$$T(\lambda) = T_{\mathrm{O_3}}(\lambda)T_{\mathrm{SO_2}}(\lambda)T_{\mathrm{NO_2}}(\lambda)T_{\mathrm{aer}}(\lambda)T_{\mathrm{ray}}(\lambda), \tag{3}$$

where $T_{\mathrm{O_3}}$, $T_{\mathrm{SO_2}}$, $T_{\mathrm{NO_2}}$, T_{aer}, and T_{ray} are the O_3, SO_2, NO_2, aerosol, and air transmittances, respectively. Each of the individual transmittances is calculated using optical depth $\tau(\lambda)$ that is the product of extinction coefficient $\beta(\lambda)$ and the ray path through the atmosphere s:

$$T(\lambda) = \exp[-\tau(\lambda)] = \exp[-\beta(\lambda)s]. \tag{4}$$

The extinction coefficient of UV radiation β is calculated as the product of the cross-sectional area σ and layer particle concentration N:

$$\beta(\lambda) = \sigma(\lambda)N. \tag{5}$$

The solar zenith angle is derived using spherical trigonometry (Spencer 1971). The optical mass, which takes into account the earth's curvature and refraction to an angle of 87°, is calculated using the formula proposed by Hiltner (1962, chapter 8). For angles between 87° and 90°, the formula from Ruggaber et al. (1994) is used. Situations in which the sun's disk is visible while its zenith angle is larger than 90° are not considered in the model. Air mass is corrected for atmospheric pressure (Bird and Riordan 1986). Different expressions for ozone optical mass are considered here because the ozone extinction process corresponds to a different vertical concentration profile (WMO 1980).

Ozone extinction cross-section values as a function of wavelength and temperature were obtained from Burrows et al. (1999) for the wavelength range 280–400 nm. Extinction cross section for SO_2 and NO_2 as a function of wavelength and temperature was obtained from Scanning Imaging Absorption Spectrometer for Atmospheric Chartography spectrometer measurements for the 280–400-nm wavelength range (Bogumil et al. 2000). Values are given for five temperatures, from 202 to 293 K, and for a particular layer estimated by a linear interpolation. The particle concentration is calculated by combining vertical profiles and total gases amount. The model uses four ozone profiles that are represen-

tative for seasons in midlatitudes, two SO_2 profiles and one NO_2 profile (Ruggaber et al. 1994).

Rayleigh extinction cross section of an air molecule is calculated using Eq. (6) (Liou 1980):

$$\sigma_r(\lambda) = \frac{8\pi^3(m_r^2 - 1)^2}{3\lambda^4 N_r^2} f(\gamma), \tag{6}$$

where m_r is the real part of refraction index, N_r is the number of molecules per cubic meter under standard conditions (2547×10^{25} m^{-3}), λ is the wavelength in micrometers, and $f(\gamma)$ is an anisotropic correction factor. Approximation of the real part of refraction index is calculated by Liou (1980), air molecule anisotropy values are used from Ruggaber et al. (1994), and particle concentration in layer is calculated using equation of state.

As mentioned previously, 10 different aerosol mixtures, which are representative of a boundary layer of certain origin from the Optical Properties of Aerosols and Clouds (OPAC; see Hess et al. 1998) model, are available in the NEOPLANTA model. These types differ one from another with regard to scattering efficiency, single scattering albedo, and asymmetry factors. The OPAC software package also gives the optical properties of upper-atmosphere aerosol, which are representative of the free troposphere (boundary layer–12 km) and stratospheric aerosol properties (12–36 km). OPAC also describes the vertical distribution of aerosol particles by an exponential profile (Hess at al. 1998). In estimating the amount of aerosols in the layer on the ground, the NEOPLANTA model provides one of the following options: (i) use of datasets supplied with the averaged values of amount of aerosols provided by the OPAC aerosol model; (ii) use of the turbidity coefficient calculated following Angstrom (1961); (iii) use of the visibility (Koschmieder 1924; Gueymard 1995); and (iv) use of the aerosol optical depth at 550 nm.

b. Diffuse radiation

The starting point for the calculation of the diffuse part of radiation is the set of equations from the spectral model described by Bird and Riordan (1986), which represents equations from previous parametric models (Leckner 1978; Brine and Iqbal 1983; Justus and Paris 1985) that were improved after comparisons with the rigorous radiative transfer model (Blattner 1983) and with measured spectra. The downward fraction is calculated from the same transmittance functions used to determine the direct beam irradiance. The diffuse irradiance is divided into three components: 1) the Rayleigh scattering component I_{ray}; 2) the aerosol scattering component I_{aer}; and 3) the component that accounts for multiple reflection of irradiance between the ground and the air I_{rf}, that is,

$$I_{\text{dif}} = I_{\text{ray}} + I_{\text{aer}} + I_{\text{rf}}. \tag{7}$$

The Rayleigh scattered component is calculated according to Bird and Riordan (1986):

$$I_{\text{ray}}(\lambda) = I_0(\lambda)T_{O_3}(\lambda)T_{SO_2}(\lambda)T_{NO_2}(\lambda)T_{\text{aa}}(\lambda) \times [1 - T_{\text{ray}}^{0.95}(\lambda)]0.5. \tag{8}$$

All the transmittance functions in Eq. (8) have been defined after Eq. (3), except the transmittance of the aerosol absorption process $T_{\text{aa}}(\lambda)$ which is defined by Justus and Paris (1985):

$$T_{\text{aa}}(\lambda) = \exp\{-[1 - \omega(\lambda)]\tau_a(\lambda)\}, \tag{9}$$

where $\omega(\lambda)$ is the single-scattering albedo, and $\tau_a(\lambda)$ is the aerosol optical thickness. Single-scattering albedo normally varies with relative humidity and wavelength and is equal to 1 for a perfectly nonabsorbing aerosol. The model NEOPLANTA uses single-scattering albedo from the OPAC database for each wavelength and humidity value.

The aerosol-scattered irradiance is calculated as

$$I_{\text{aer}}(\lambda) = I_0(\lambda)T_{O_3}(\lambda)T_{SO_2}(\lambda)T_{NO_2}(\lambda)T_{\text{aa}}(\lambda)T_{\text{ray}}^{1.5}(\lambda) \times [1 - T_{\text{as}}(\lambda)]D_s(\lambda), \tag{10}$$

where $T_{\text{as}}(\lambda)$ is the transmittance for aerosol scattering, such that

$$T_{\text{aa}}(\lambda) = \exp[-\omega(\lambda)\tau_a(\lambda)], \tag{11}$$

and D_s is the fraction of the scattered flux that is transmitted downward. According to Bird and Riordan (1986) and Justus and Paris (1985), the function D_s is dependent on the aerosol asymmetry factor δ as

$$D_s = F_s C_s, \tag{12}$$

$$F_s = 1 - 0.5 \exp[(B_1 + B_2 \cos\theta)\cos\theta], \tag{13}$$

$$B_1 = B_3[1.459 + B_3(0.1595 + B_3 0.4129)], \tag{14}$$

$$B_2 = B_3[0.0783 + B_3(-0.3824 - B_3 0.5874)], \tag{15}$$

$$B_3 = \ln(1 - \delta), \quad \text{and} \tag{16}$$

$$C_s(\lambda) = (\lambda + 0.55)^{1.8}. \tag{17}$$

The asymmetry factor is a key optical characteristic of aerosols and it is used from the OPAC database for each wavelength and humidity value.

The backscattered component of multiple reflections between the air and ground is calculated according to Bird and Riordan (1986):

$$I_{\mathrm{rf}}(\lambda) = \frac{[I_{\mathrm{dir}}(\lambda) + I_{\mathrm{ray}}(\lambda) + I_{\mathrm{aer}}(\lambda)]r_s(\lambda)r_g(\lambda)C_s(\lambda)}{1 - r_s(\lambda)r_g(\lambda)}, \tag{18}$$

where $r_g(\lambda)$ is ground albedo and $r_s(\lambda)$ is sky reflectivity. The ground albedo is used from Ruggaber et al. (1994), while sky reflectivity is calculated by

$$r_s(\lambda) = T'_{\mathrm{O_3}}(\lambda)T'_{\mathrm{aa}}(\lambda)\{0.5[1 - T'_{\mathrm{ray}}(\lambda)] + [1 - F'_s(\lambda)]T'_{\mathrm{ray}}(\lambda)[1 - T'_{\mathrm{as}}(\lambda)]\}, \tag{19}$$

where the primed transmittance terms are the regular atmospheric transmittance evaluated at optical mass of 1.8.

c. Biologically active UV radiation and UV index

The UV index (UVI) describes the potential erythemal effects of UV radiation on human skin. A unit of UVI corresponds to 0.025 W m^{-2} of biologically active UV radiation UV_{bio} and is defined according to McKenzie et al. (2003) as

$$\mathrm{UVI} = \mathrm{UV_{bio}} \times 40. \tag{20}$$

The potential biologically active UV irradiance at the surface is found by the multiplication of the UV spectrum and the action spectrum and integration between 280 and 400 nm:

$$\mathrm{UV_{bio}} = \int_{280}^{400} B(\lambda)I(\lambda)\,d\lambda, \tag{21}$$

where $B(\lambda)$ is normalized erythemal action spectrum and $I(\lambda)$ is spectral UV irradiance (direct + diffuse). To calculate the biologically effective of UV radiation, the spectral UV irradiance is weighted by the erythemal action spectrum $B(\lambda)$by McKinley and Diffey (1987) as

$$B(\lambda) = \begin{cases} 1 & \text{for} \quad \lambda < 298 \text{ nm} \\ 10^{0.094(298-\lambda)} & \text{for} \quad 298 \text{ nm} < \lambda < 328 \text{ nm} \\ 10^{0.015(139-\lambda)} & \text{for} \quad 328 \text{ nm} < \lambda < 400 \text{ nm} \\ 0 & \text{for} \quad \lambda > 400 \text{ nm} \end{cases}. \tag{22}$$

3. Model evaluation

The performance of the model was tested by comparing UVI values of the model outputs with measurements recorded with a Yankee UVB-1 biometer (see Yankee Environmental Systems, Inc. 2000). For the test, we have selected data for 10 days, measured in the years 2003, 2004, and 2005, with cloudiness less than 0.2.

The device is located at the Novi Sad University campus (45.33°N, 19.85°E; 84 m MSL). This biometer detects UV radiation every 10 s, but our measurements were collected with a temporal resolution of 10 min. The main sources of errors in UVI measurements are uncertainties in the determination of the calibration constant of the instrument and the conversion of the analog signal at the output of the instrument to a digital one (error of quantization). Because measurements in this paper are expressed in UVI units, an additional source of error is uncertainty of the factor that is used to convert integrated spectral data (W m^{-2}) to erythemal weighted irradiance (McKinley and Diffey 1987). The Yankee UVB-1 biometer was calibrated in 2002 at the factory (Yankee Environmental Systems, Inc. 2002) using the National Institute of Standards and Technology–traceable reference detector and appropriate equipment. Because results presented here are from the 2003–05 period, it is reasonable to accept this calibration as reliable, assuming long-term stability of the instrument. According to the user guide (Yankee Environmental Systems, Inc. 2000), the upper limit of error for the calibration constant is 8%, while the conversion to erythemal weighted irradiance introduces an error of about 4% (for a solar zenith angle lower than 65°). The quantization error can be neglected, because a precise 12-bit analog-to-digital converter is used to convert the analog signal (0–4 V) from the instrument into the digital form. Taking into account the aforementioned errors, the estimated maximal error of the measurements is less than 9%.

The UVI was calculated by the model every half hour from sunrise to sunset. In the model calculations we considered the effects of O_3, aerosols, and ground surface type on UVI. Effects of SO_2 and NO_2 were not taken into account because of their low impact on UVI (Forster et al. 1995; Zeng et al. 1994). The total column ozone in the atmosphere is the input parameter that has to be known. The total column ozone over the Novi Sad coordinates for the considered days was taken from the online database of the Total Ozone Mapping Spectrometer Earth Probe observations (NASA 2005). There exist no measurements of aerosol chemical composition and amount in Novi Sad, so we considered aerosol to be the main source of difference between measured and calculated values. Because of a large portion of soil particles and soot presence in the air of the town, the continental averaged aerosol type is assumed. Aerosol extinction is calculated taking visibility data at 1200 UTC from SYNOP data files and using the equation by Koschmieder (1924). For simplicity, ozone and aerosol levels were assumed to be constant over the day. The surface albedo was fixed for each surface type considered. Figure 1 depicts the comparison between the cal-

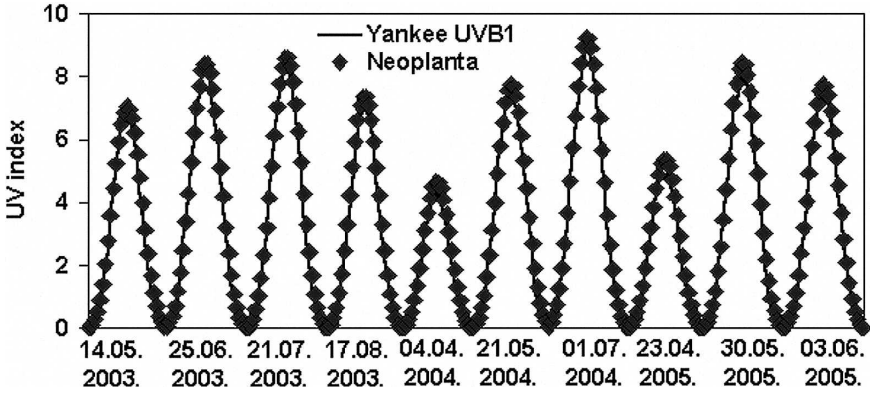

FIG. 1. Variation of the UVI obtained by the NEOPLANTA model in comparison with the observations in Novi Sad for cloudless days.

culated diurnal variations of UVI for cloudless days in 2003, 2004, and 2005. From this figure, it is seen that the NEOPLANTA model gives the values that are very close to the observations. This fact is more visualized in Fig. 2, where the modeled values are plotted against the observations. Note that model and model parameter uncertainties affect the calculated values. For the model presented in this analysis, more details can be found in Malinovic (2003).

To quantify the modeled values of UVI, we have performed an error analysis of the outputs obtained. Following this, we computed several statistical quantities as follows (Pielke 2002; Mihailovic et al. 2004):

$$\nu = \left[\frac{1}{N}\sum_{i=1}^{N}(\Gamma_i - \hat{\Gamma}_i)^2\right]^{1/2}, \tag{23}$$

$$\nu_{\mathrm{BR}} = \left\{\frac{1}{N}\sum_{i=1}^{N}[(\Gamma_i - \overline{\Gamma}) - (\hat{\Gamma}_i - \overline{\hat{\Gamma}})]^2\right\}^{1/2}, \tag{24}$$

$$\eta = \left[\frac{1}{N}\sum_{i=1}^{N}(\Gamma_i - \overline{\Gamma})^2\right]^{1/2}, \tag{25}$$

and

$$\hat{\eta} = \left[\frac{1}{N}\sum_{i=1}^{N}(\hat{\Gamma}_i - \overline{\hat{\Gamma}})^2\right]^{1/2}. \tag{26}$$

Here, Γ is the variable of interest (UVI in this study), while N is the total amount of data. An overbar indicates the arithmetic average, while a caret refers to an observation. The absence of a caret indicates a modeled value. Further, ν is the root-mean-square error (rmse), while ν_{BR} is the rmse after a bias is removed. Root-mean-square errors give a good overview of a dataset, with large errors weighted more than many small errors (Mahfouf 1990). The standard deviations in the simulation and the observations are given by η and $\hat{\eta}$, respectively. An rmse that is less than the standard deviation of the observed value indicates quality in the simulation. Moreover, the values of η and $\hat{\eta}$ should be close if the prediction is to be considered realistic. The statistics for the values of the UVI used are listed in Table 1. It indicates that the rmse is less than the standard deviation of the observed values. Also, a comparison of η (2.78) and $\hat{\eta}$ (2.71) shows that the difference between them is very small. This analysis shows that the modeled values of UVI agree well with the observations.

We also made a comparison between the modeled and the measured values under the following quantities: (i) the percentage difference between model esti-

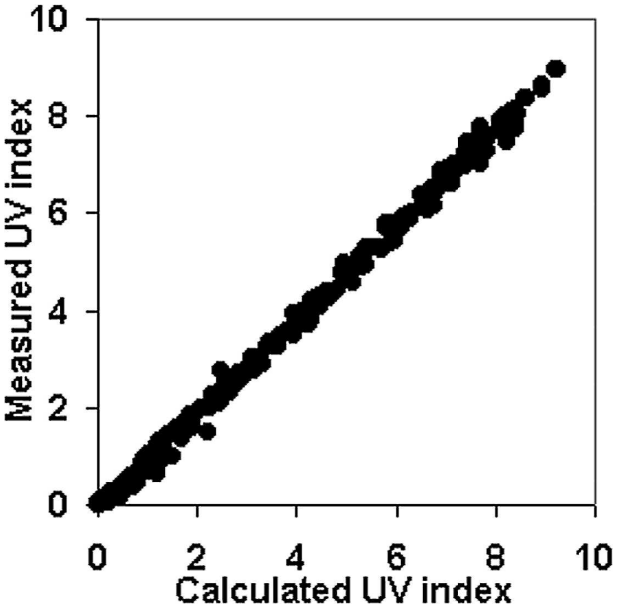

FIG. 2. The UVI obtained by the NEOPLANTA model plotted against the observations recorded in Novi Sad for cloudless days.

TABLE 1. Error analysis of the modeled UVI.

Statistical parameters from Eqs. (23)–(26)			
ν	ν_{BR}	η	$\hat{\eta}$
0.25	0.15	2.78	2.71

mations and measurements (PDEM) defined as PDEM = $\{\Gamma - \hat{\Gamma}\}/\Gamma$, where a caret refers to an observation; and (ii) the absolute difference between model estimations and measurements (ADEM) defined as ADEM = $|\Gamma - \hat{\Gamma}|$. Larger values of the PDEM are expected for higher values of the solar zenith angle, because the corresponding larger values of air mass introduce more significant differences between modeled and measured values of UVI. Figure 3 depicts the percentage difference between the model estimations and measurements (PDEM) with respect to the solar zenith angle. From this figure, it is seen that the agreement between the modeled and measured values is better for lower solar zenith angles. A simple statistical overview of Fig. 3 indicates that 87% of the samples have a PDEM of less than 10%, for the solar zenith angles lower than 60°. Last, the ADEM values show that 95% of the absolute differences are in the interval of ±0.5 UVI.

4. Concluding remarks

In this work we presented a numerical model called NEOPLANTA, designed at the University of Novi Sad, for estimating the solar UV irradiance and UVI under cloud-free conditions. This model, including the effects of O_3, SO_2, NO_2, aerosols, and nine different ground surface types on UV radiation, computes the direct solar and diffuse UV irradiances for the wavelength range 280–400 nm, and gives the values of UVI. To examine how well the model designed supports simulations, a test was performed using model outputs of UVI for 10 spring and summer days (the years 2003, 2004, and 2005). They were compared with data recorded by the Yankee UVB-1 biometer located at the university campus in Novi Sad, Serbia. Error analysis shows that the modeled values of UVI agree well with the observations. In further development of the model, we plan (i) to establish, over the sensitivity tests, how model and model parameter uncertainties affect the UVI and (ii) to use this as a forecasting model including the outputs from the ozone and atmospheric prediction models.

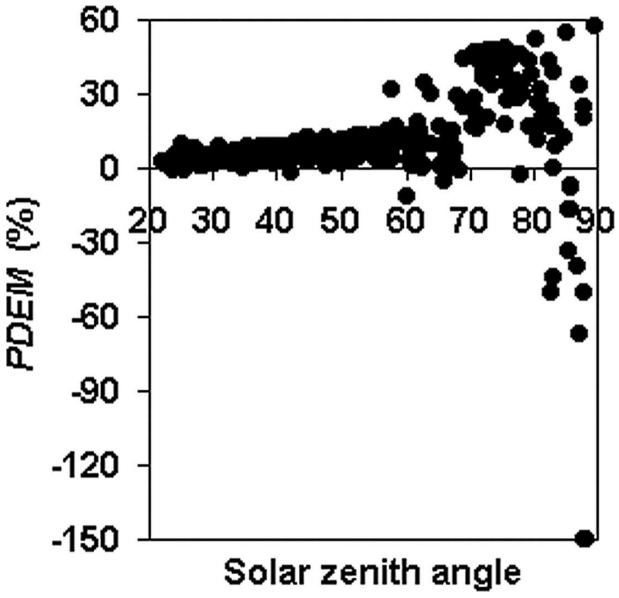

FIG. 3. The PDEM with respect to the solar zenith angle. Data are from Fig. 1.

Acknowledgments. The research work described in this paper has been funded by the Serbian Ministry of Science and Environmental Protection under the project "Modeling and numerical simulations of complex physical systems," ON141035 for 2006-2010. The authors thank Mr. Vladimir Skoric for proofreading the paper.

REFERENCES

Angstrom, A., 1961: Technique of determining the turbidity of the atmosphere. *Tellus,* **13,** 214–231.

Bird, R. E., and C. Riordan, 1986: Simple solar spectral model for direct and diffuse irradiance on horizontal and titled planes at the earth's surface for cloudless atmosphere. *J. Climate Appl. Meteor.,* **25,** 87–97.

Blattner, W., 1983: Utilization instruction for the BRITE Monte-Carlo procedure. Radiation Research Associates, Fort Worth, TX, 104 pp.

Bogumil, K., J. Orphal, and J. P. Burrows, 2000: Temperature dependent absorption cross section of O_3, NO_2 and other atmospheric trace gases measured whit SCIAMACHY spectrometer. *Proc. ERS- ENVISTAT Symp.,* Gothenburg, Sweden, ESA–ESTEC, 11 pp. [Available online at http://earth.esa.int/pub/ESA_DOC/gothenburg/099bogum.pdf.]

Brine, D. T., and M. Iqbal, 1983: Solar spectral diffuse irradiance under cloudless skies. *Sol. Energy,* **30,** 447–453.

Burrows, J. P., A. Richter, A. Dehn, B. Deters, S. Himmelmann, S. Voigt, and J. Orphal, 1999: Atmospheric remote sensing reference data from GOME—2. Temperature-dependent absorption cross section of O3 in the 231–794 nm range. *J. Quant. Spectrosc. Radiat.,* **61,** 509–517.

Burrows, W. R., M. Vallee, D. I. Wardle, J. B. Kerr, L. J. Wilson, and D. W. Tarasick, 1994: The Canadian operational procedure for forecasting total ozone and UV radiation. *Meteor. Appl.,* **1,** 247–265.

Diffey, B. L., 1977: The calculation of the spectral distribution of natural ultraviolet radiation under clear day conditions. *Phys. Med. Biol.,* **22,** 309–316.

Forster, P., K. P. Shine, and A. R. Webb, 1995: Modeling ultraviolet radiation at the earth's surface. Part II: Model and instrument comparison. *J. Appl. Meteor.,* **34,** 2426–2439.

Glandorf, M., A. Arola, A. Bais, and G. Seckmeyer, 2005: Possibilities to detect trends in spectral UV irradiance. *Theor. Appl. Climatol.,* **81,** 33–44.

Gueymard, C., 1995: SMARTS, A Simple Model of the Atmospheric Radiative Transfer of Sunshine: Algorithms and performance assessment. Florida Solar Energy Center Tech. Rep. FSEC-PF-270-95, 78 pp.

Hess, M., P. Koepke, and I. Schult, 1998: Optical properties of aerosols and clouds: The software package OPAC. *Bull. Amer. Meteor. Soc.,* **79,** 831–844.

Hiltner, W. A., 1962: *Stars and Stellar Systems: Compendium of Astronomy and Astrophysics.* Vol. II., The University of Chicago Press, 180 pp.

Justus, C. G., and M. V. Paris, 1985: A model for solar spectral irradiance at the bottom and top of a cloudless atmosphere. *J. Climate Appl. Meteor.,* **24,** 193–205.

Kneizys, F. X., E. P. Shettle, L. W. Abreu, J. H. Chetwynd, G. P. Anderson, W. O. Gallery, J. E. A. Selby, and S. A. Clough, 1988: LOWTRAN 7. Tech. Rep. AFGL-TR-88-0177, Environmental Research Papers 1010, 146 pp.

Koepke, P., and Coauthors, 1998: Comparison of models used for UV index calculations. *Photochem. Photobiol.,* **67,** 657–662.

Koschmieder, H., 1924: Theorie der horizontalen Sichtweite (Theory of horizontal visibility). *Beitr. Phys. Atmos.,* **12,** 33–53.

Leckner, B., 1978: The spectral distribution of solar radiation at the earth's surface—Elements of a model. *Sol. Energy,* **20,** 143–150.

Liou, K. N., 1980: *An Introduction to Atmospheric Radiation*. Academic Press, 392 pp.

Madronich, S., L. O. Björn, M. Ilyas, and M. M. Caldwell, 1998: Changes in biologically active ultraviolet radiation reaching the earth's surface. *J. Photochem. Photobiol. B,* **46,** 5–19.

Malinovic, S., 2003: A model for the prognosis of the intensity of UV radiation using the numerical weather prediction model. M.S. thesis, University of Novi Sad, 103 pp. [Available from Association of Centers for Interdisciplinary and Multidisciplinary Studies and Developmental Research, Trg Dositeja Obradovica 5, 21000 Novi Sad, Serbia.]

Mahfouf, J. F., 1990: A numerical solution of the surface water budget during HAPEX MOBILHY. *Bound.-Layer Meteor.,* **53,** 201–222.

McKenzie, R. L., L. O. Björn, A. Bais, and M. Ilyasd, 2003: Changes in biologically active ultraviolet radiation reaching the earth's surface. *Photochem. Photobiol. Sci.,* **2,** 5–15.

McKinley, A. F., and B. L. Diffey, 1987: A reference action spectrum for ultraviolet induced erythema in human skin. *CIE J.,* **6,** 17–22.

Mihailovic, D. T., K. Alapaty, B. Lalic, I. Arsenic, B. Rajkovic, and S. Malinovic, 2004: Turbulent transfer coefficients and calculation of air temperature inside the tall grass canopies in land–atmosphere schemes for environmental modeling. *J. Appl. Meteor.,* **43,** 1498–1512.

NASA, cited 2005: Total Ozone Mapping Spectroradiometer. [Available online at http://toms.gsfc.nasa.gov/.]

Pielke, R. A., Sr., 2002: *Mesoscale Meteorological Modeling*. 2d ed. Academic Press, 676 pp.

Rozanov, V. V., D. Diebel, R. J. D. Spurr, and J. P. Burrows, 1997: GOMETRAN: A radiative transfer model for the Satellite project GOME—The plane parallel version. *J. Geophys. Res.,* **102** (D14), 16 683–16 695.

Ruggaber, A., R. Dlugi, and T. Nakajima, 1994: Modeling of radiation quantities and photolysis frequencies in the troposphere. *J. Atmos. Chem.,* **18,** 171–210.

Schwander, H., A. Kaifel, A. Ruggaber, and P. Koepke, 2001: Spectral radiative transfer modeling with minimized computation time using neural network technique. *Appl. Opt.,* **40,** 331–335.

Spencer, J. W., 1971: Fourier series representation of the position of the sun. *Search,* **2,** 172–173.

WMO, 1980: Operations handbook—–Ozone observations with a Dobson spectrophotometer. Global Ozone Research and Monitoring Project 6, Geneva, Switzerland, 125 pp.

——, 1997: Report of the WMO–WHO meeting of experts on standardization of UV indices and their dissemination to the public. WMO GAW 127, WMO Tech. Doc. 921, Les Diablerets, 187 pp.

——, 2003: Scientific assessment of ozone depletion: 2002. Global Ozone Research and Monitoring Project, 47 (5), Geneva, Switzerland, 49 pp.

Yankee Environmental Systems, Inc., 2000: *UVB-1 UV Pyranometer, Installation and User Guide, version 2.0*. 44 pp.

——, 2002: *Certificate of Calibration.* 1 p.

Zeng, J., R. McKenzie, K. Stamnes, M. Wineland, and J. Rosen, 1994: Measured UV spectra compared with discrete ordinate method simulations. *J. Geophys. Res.,* **99** (D11), 23 019–23 030.

Zerefos, C. S., 2002: Long-term ozone and UV variations at Thessaloniki, Greece. *Phys. Chem. Earth,* **27,** 455–460.